Revisiting the Nature of Adsorption and Desorption Branches: Temperature Dependence of Adsorption Hysteresis in Ordered Mesoporous Silica

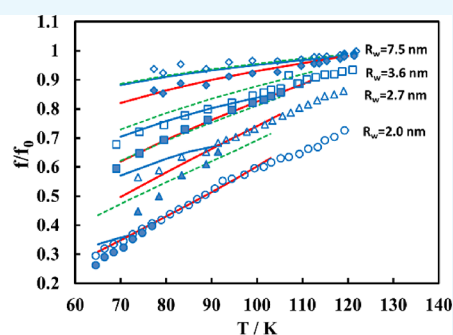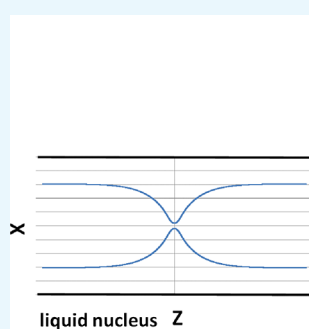Kunimitsu Morishige*

Read Online

ACCESS | Metrics & More | Article Recommendations

ABSTRACT: To gain a deeper understanding as to the nature of the adsorption hysteresis due to capillary condensation of nitrogen in ordered mesoporous silicas, we calculated the temperature dependences of the activated condensation, equilibrium transition, and activated desorption pressures for nitrogen in spherical and cylindrical silica pores with several different pore sizes on the basis of semimacroscopic continuum models. The results clearly indicate that the models capture the exact nature of capillary condensation and evaporation phenomena of a fluid in cagelike and cylindrical mesopores. The temperature dependences of the adsorption hysteresis of nitrogen measured confirm previous theoretical predictions for cylindrical pores: for the ordered mesoporous silicas with cylindrical mesopores at least greater than ∼7 nm in diameter, the capillary condensation takes place via a nucleation process followed by a growth process of a bridging meniscus at pressures higher than the equilibrium transition, while the capillary evaporation takes place via a receding meniscus from pore ends at the equilibrium. For SBA-15 and MCM-41 with smaller mesopore sizes, on the other hand, the capillary condensation takes place close to the equilibrium transition pressures, while the capillary evaporation takes place at pressures lower than the equilibrium, owing to single pore blocking due to corrugation of the cylindrical pores. We discuss the effect of curvature on surface tension in capillary condensation, as well as the relation between a change in the mechanisms of adsorption and desorption and the pore corrugation in the cylindrical pores.

1. INTRODUCTION

Mesopores with diameters in the range of 2−50 nm are formed in a wide variety of materials such as bulk powder,[1] colloidal crystal,[2] concrete,[3] and shale.[4] When these mesoporous materials are exposed to a vapor at a pressure less than the saturation pressure (p_0) of the bulk liquid, capillary condensation of the vapor takes place to form a liquid-like phase in the mesopores.[4−9] The phenomenon is concerned with lubrication, adhesion, and agglomeration and widely utilized in the characterization of porous materials. Capillary condensation of various subcritical fluids is very often accompanied by hysteresis in the adsorption−desorption isotherm. The nature of adsorption and desorption branches is still a long-standing problem in capillary condensation because it is directly concerned with a proper pore size analysis of the mesoporous materials.[5,8]

Theoretical and simulation studies[6,10−13] strongly suggest that the origin of the hysteresis is dependent on the pore geometry at the level of a single pore. Among various pore geometries that may be considered, cylindrical and ink-bottle geometries are especially important because the pore structures of the mesoporous materials can be often mimicked by these two geometries or the connection of these geometries.[10−18] In an open-ended cylindrical pore,[6,10,12] the hysteresis arises from the formation of a metastable multilayer film on the pore walls upon

adsorption, while desorption takes place via a receding meniscus at an equilibrium transition pressure because capillary evaporation does not involve nucleation. In an ink-bottle pore composed of a wide pore (cavity) surrounded by narrower cylindrical pores (necks),[6,11,13] a metastable multilayer film on the walls of the wide pore is formed upon adsorption. The shape of the wide pore may be spherical or cylindrical. Desorption no longer takes place at the equilibrium, and a fluid condensed in the wide pore shows large metastability. The desorption mechanism changes with the size of the narrow necks.[19] If the neck diameter is not too small, the desorption of a fluid in the wide pore takes place with the desorption of a fluid condensed in the narrow neck (pore blocking effect). In a network of the ink-bottle pores, the desorption is controlled by the size and spatial distribution of the necks. The network may empty at a relative pressure (p/p_0) corresponding to a characteristic percolation threshold.[14−16] When the neck diameter is smaller than a certain characteristic size, the desorption from the wide pore takes place via diffusion through the narrow necks and the fluid in the necks remains condensed (cavitation). In any case, the extent of the metastability on desorption is significantly larger than that on adsorption.

On the other hand, experimental verification of these theoretical predictions concerning the nature of the adsorption hysteresis is not necessarily easy because the equilibrium transition pressure within the hysteresis region is usually difficult to be estimated without the help of a heavy calculation work.[6,12,13] In previous studies, we proposed a useful method to examine experimentally the nature of the adsorption hysteresis.[20,21] The width of the hysteresis decreases with increasing temperature and eventually the hysteresis disappears at a certain temperature T_h called the *hysteresis temperature*. The principle of the method is simple; that is, the equilibrium pressure of capillary condensation inside the hysteresis loop can be obtained by the extrapolation of the reversible condensation pressures measured at higher temperatures to lower temperatures at which the adsorption hysteresis is observed. The experimental results for SBA-16 and KIT-5 ordered mesoporous silicas with spherical pores were nearly consistent with the theoretical predictions mentioned above.[22,23] The experimental results for MCM-41 and SBA-15 ordered mesoporous silicas with cylindrical pores, however, did not necessarily agree with the theoretical predictions.[20,21,24,25] The origin of inconsistency was thought to be due to imperfections of pore geometry.[25] Although such an extrapolation method is intuitive and useful, it still has no support from a theoretical framework.

For an open-ended cylindrical pore, a number of macroscopic thermodynamic models have been reported: they give estimates of both the equilibrium phase transition pressure and spontaneous capillary condensation pressure at the limit of stability of the metastable adsorption film.[26−38] These models differ with each other in the attractive potential from the pore wall and the dependency of the surface tension on curvature. Microscopic nonlocal density functional theory (NLDFT) is also capable to give estimates of the spontaneous capillary condensation pressure at the limit of stability of the adsorbed film, as well as the equilibrium transition pressure.[39] However, all these models are not capable to give an exact estimate of the capillary condensation pressure because capillary condensation does not necessarily occur at the limit of stability of the adsorbed film, namely, at the vaporlike spinodal.[12,39,40] Capillary condensation takes place by nucleation at a certain critical pressure between the equilibrium and the vaporlike spinodal,

which depends on the height of the energy barrier separating the metastable and stable states.[12,40] Similarly, molecular simulations are not capable to give a reasonable estimate of the capillary condensation pressure because the density and energy fluctuations in the molecular simulations are far smaller than those in realistic systems.[40] Very recently, Hiratsuka, Tanaka, and Miyahara (HTM),[41] and Bonnet and Wolf (BW)[42] proposed semimacroscopic models that can give reasonable estimates of both the equilibrium phase transition pressure and capillary condensation pressure from a metastable state for a fluid in an open-ended cylindrical pore without computationally expensive molecular simulations. These models allow us to estimate the hysteresis temperature, too.

A molecular simulation study[40] has confirmed the Everett−Haynes scenario[43] that capillary condensation of a fluid in an open-ended cylindrical pore proceeds via bridging through the formation of a bump/undulation on the adsorption film. When capillary evaporation from pore ends at equilibrium is forbidden, it may occur via cavitation. The BW model is capable of reproducing both the vapor-to-liquid nucleation via bridging and the liquid-to-vapor nucleation via cavitation in the framework of the semimacroscopic continuum model. The curve of the nucleation barrier versus chemical potential obtained by this phenomenological model was similar to that obtained by the microscopic molecular simulations.[42] The adsorption hysteresis at a given temperature is expected when the nucleation barrier at the vapor−liquid equilibrium (VLE), which is a progressively increasing function of the pore size, becomes insurmountable. The hysteresis for a given pore size disappears when the nucleation barrier at the VLE becomes surmountable with increasing temperature. The disappearance of hysteresis above T_h has a dynamic rather than a thermodynamic nature. The level of surmountable nucleation barrier at given experimental conditions is thought to depend on both the degree of approximations used in the estimation of the nucleation barrier and the experimental conditions such as inevitable temperature fluctuations. Therefore, the level of surmountable nucleation barrier cannot be determined in advance.

The mechanism of nucleation in a spherical pore is straightforward, and the estimation of the nucleation barrier from a classic thermodynamic model is simple.[44] The ordered mesoporous silicas inevitably have pore imperfections such as undulations and constrictions to some extent depending on the synthesis method. However, it is expected that such pore imperfections do not at all affect the mechanism of nucleation in the spherical pore, as opposed to that in the cylindrical pore. The height of the nucleation barrier for the cavitation changes more gradually with chemical potential as compared to that for capillary condensation. Therefore, the pressure of cavitation-induced desorption calculated is significantly influenced by the level of surmountable nucleation barrier selected. Reversely, this allows us to determine the proper level of surmountable nucleation barrier from a comparison between the temperature dependence of capillary evaporation (cavitation) pressure observed for the ordered mesoporous silicas with cagelike pores and those calculated. The temperature dependences of cavitation pressure were calculated based on the semimacroscopic model for several different levels of the surmountable nucleation barrier. With this knowledge about the level of the surmountable nucleation barrier, the capillary condensation and evaporation pressures as well as T_h for a fluid in cylindrical pores can be calculated with more precision. The nature of the

adsorption hysteresis observed for the ordered mesoporous silicas with cagelike and cylindrical pores can be examined more correctly from a comparison between the experimental and theoretical temperature dependences of the hysteresis. Especially, the nature of adsorption and desorption branches in adsorption isotherms is very important in relation to the pore size analysis of the mesoporous materials.[5,8]

The present study aims at elucidating the nature of the adsorption hysteresis of nitrogen for the ordered mesoporous silicas MCM-41 and SBA-15 with cylindrical pores from a comparison between the temperature dependence of the adsorption hysteresis observed in experiments and that obtained theoretically for an ideal cylindrical pore. This gives a theoretical support to our examination method as to the nature of the adsorption and desorption branches in the hysteretic adsorption isotherms. The theoretical calculations based on the continuum thermodynamic model will complement the temperature dependence of adsorption hysteresis measured and lead to more reliable conclusions as to the nature of the adsorption and desorption branches observed. Here, the experimental data are taken from our previous studies concerning nitrogen adsorption in the cagelike and cylindrical pores of the ordered mesoporous silicas MCM-41,[23,24] SBA-15,[23,24] SBA-16,[23] KIT-5,[23] and SBA-12.[23]

2. RESULTS AND DISCUSSION

2.1. Spherical Pore. When the necks of an inkbottle pore are smaller than a certain critical size, the capillary evaporation of a fluid condensed inside the wide pore takes place via cavitation.[19] The ordered mesoporous silicas with cagelike pores usually reveal cavitation-induced desorption.[13,22,23,44,45] Therefore, both the capillary condensation and evaporation take place by thermally activated nucleation. The rate of the thermally activated nucleation is usually given by the Arrhenius law. It is well-known that the essential variation in the nucleation rate comes from the exponential factor. The variation of the prefactor with temperature and pore size is negligibly small compared to that of the exponential factor. If the present continuum model captures the exact nature of capillary condensation and evaporation of a fluid in an inkbottle pore, the model will be capable of reproducing the capillary condensation and evaporation pressures observed for various temperatures and pore sizes using a single value of the dimensionless level of surmountable nucleation barrier, $N_c = E^*/k_b T$, where k_b is the Boltzmann constant.[42,46] We calculated the nucleation barrier (E^*) for activated capillary condensation and evaporation as a function of relative fugacity pressure (f/f_0) at several different temperatures for nitrogen in a spherical pore of $R_w = 7.0$ nm. Here, R_w is a distance between the surface of the pore wall and the pore center. The curve of E^* versus f/f_0 was asymmetrical, and the maximum was attained at VLE, in accord with previous molecular simulation studies.[47,48] The barrier height for evaporation gradually decreases with deceasing f/f_0, while the barrier height for condensation rapidly decreases with increasing f/f_0. This implies that the capillary evaporation pressure calculated is significantly affected by the value of N_c selected, whereas the capillary condensation pressure calculated is affected little by it. Figure 1 shows a comparison of the temperature dependences of capillary condensation and evaporation pressures (f/f_0) for nitrogen in KIT-5 (expand) with the calculated temperature dependences. The calculated ones were obtained based on the semimacroscopic model assuming four different values of $N_c = 40$, 50, 60, and 70. A
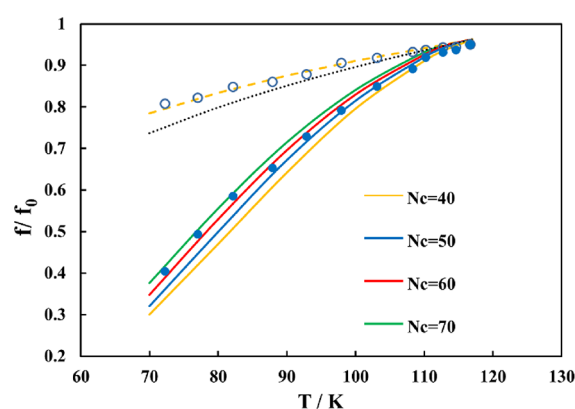

Figure 1. Temperature dependence of the capillary condensation and evaporation pressures (f/f_0) of nitrogen in KIT-5 (expand). Open and closed circles denote capillary condensation and evaporation pressures, respectively. Broken, dotted, and full lines denote the capillary condensation, equilibrium transition, and cavitation pressures, respectively, of nitrogen calculated on the basis of the semimacroscopic model with no size effect in surface tension for a spherical pore. Cavitation pressures are estimated on the basis of four different levels of surmountable nucleation barrier of $N_c = 40$, 50, 60, and 70, which are denoted by yellow, blue, red, and green lines, respectively.

selection of $N_c = 60$ gives a best fit with the cavitation pressures for nitrogen on KIT-5 (expand). On the other hand, the capillary condensation pressure did not appreciably change with different values of N_c: the change is small compared with the symbol. We will fix the value of N_c at 60 hereafter.

Figure 2 shows a comparison of the temperature dependences[23] of capillary condensation and evaporation pressures for
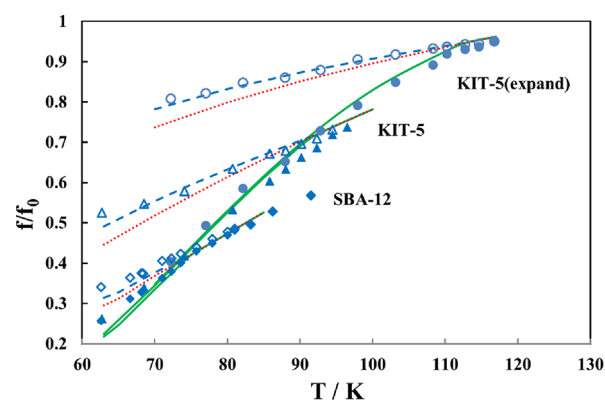

Figure 2. Temperature dependence of the capillary condensation and evaporation pressures (f/f_0) of nitrogen in SBA-12, KIT-5, and KIT-5 (expand). Open and closed symbols denote capillary condensation and evaporation pressures, respectively. Blue broken, red dotted, and green full lines denote the capillary condensation, equilibrium transition, and cavitation pressures, respectively, of nitrogen calculated on the basis of the semimacroscopic model with no size effect in surface tension for a spherical pore.

nitrogen in KIT-5 (expand), KIT-5, and SBA-12 with those calculated based on the model. The temperature dependence of the equilibrium transition pressure calculated is also included in the figure. In these calculations, pore radii of KIT-5 (expand), KIT-5, and SBA-12 were assumed to be 7.0, 3.7, and 2.7 nm, respectively. A fit between experiment and theory is excellent for KIT-5 (expand) and KIT-5, whereas SBA-12 with the smaller cavity size shows slight deviations between experiment and

theory at lower temperatures. For SBA-12, the capillary condensation and evaporation pressures calculated become progressively lower than the experimental pressures with decreasing temperature. This indicates that the present continuum model captures the exact nature of capillary condensation and evaporation phenomena for a fluid in cagelike pores at least greater than ~7 nm in diameter. The model assumes that the density and surface tension of the adsorbed multilayer film on the pore walls are equal to the density and surface tension of a bulk liquid, respectively. The dependence of surface tension on the curvature of the liquid−vapor interface, on the contrary, has been often taken into account in the modeling of capillary condensation based on the continuum approach.[30−34,36,38,41] The results clearly indicate that the effect of curvature on surface tension is not appreciably important at least for mesopores with diameters above ~7 nm.

2.2. Cylindrical Pore. For an open-ended cylindrical pore, previous theoretical and simulation studies strongly suggest that capillary condensation takes place from a metastable state of multilayer film by an activated process, while capillary evaporation takes place via a receding meniscus from pore ends at the equilibrium transition pressure.[6,10,12,39,40] If capillary evaporation at the equilibrium is inhibited, pore-blocking or cavitation-controlled desorption will occur from a metastable liquidlike state. Figure 3 shows a comparison of the temperature
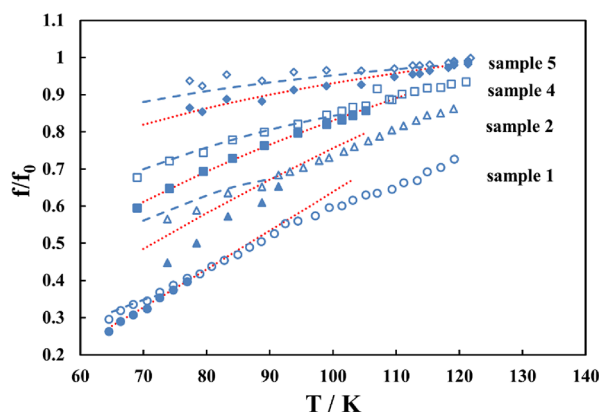

Figure 3. Temperature dependence of the capillary condensation and evaporation pressures (f/f_0) of nitrogen in MCM-41 (sample 1), SBA-15 (sample 2), SBA-15 (sample 4), and SBA-15 (sample 5). Open and closed symbols denote capillary condensation and evaporation pressures, respectively. Blue broken and red dotted lines denote the capillary condensation and equilibrium transition pressures, respectively, of nitrogen calculated on the basis of the semimacroscopic model with no size effect in surface tension for a cylindrical pore.

dependences[24] of capillary condensation and evaporation pressures of nitrogen in MCM-41 (sample 1), SBA-15 (sample 2), SBA-15 (sample 4), and SBA-15 (sample 5) with cylindrical pores with those calculated based on the model. Samples 2 and 4 were prepared using a Pluronic 123 triblock copolymer as a structure-directing agent at aging temperatures of 323 and 373 K, respectively. It is known that low aging temperatures lead to the lowering of both pore size and pore structural regularity.[49] Sample 5 was prepared using mesitylene as a solubilizing agent and P123 surfactant at an aging temperature of 373 K, in order to obtain SBA-15 with large mesopores. In the calculations, the pore radii of samples 1, 2, 4, and 5 were assumed to be 2.0, 2.7, 3.6, and 7.5 nm, respectively. For samples 4 and 5, the capillary condensation and evaporation pressures observed nicely agree

with the temperature dependences of the activated condensation and equilibrium transition pressures calculated, respectively. This confirms the conclusions of the theoretical studies mentioned above for the ordered mesoporous silicas with cylindrical mesopores at least greater than ~7 nm in diameter.

However, the results for sample 2 do not agree with the theoretical predictions for a cylindrical pore. The capillary evaporation pressures observed significantly deviate from the temperature dependence of the equilibrium transition pressure calculated, as opposed to samples 4 and 5. This is thought to be due to pore imperfections of this material and perhaps the enhanced pore corrugation of the SBA-15 sample. The amplitude of pore corrugation of sample 2 is expected to be much larger than for samples 4 and 5 because sample 2 was prepared at a low aging temperature.[50] For sample 1, the reversible capillary condensation pressures observed show systematic deviations at higher temperatures from the temperature dependence of the equilibrium transition pressure calculated: the equilibrium transition pressure calculated becomes progressively higher than the reversible condensation pressure observed with increasing temperature. The combined results for MCM-41 and SBA-12 with small mesopores indicate that the ratio between the calculated and observed transition pressures reverses at around 80 K. It is known, on the other hand, that the equilibrium capillary condensation pressure obtained by the modeling increases as the surface tension at the interface between the vapor and adsorbed phases decreases.[41] This implies that in small mesopores, the effect of curvature on the surface tension is recognizable and the ratio of the surface tensions between the confined phase and the flat surface reverses with temperature.

2.3. Pore-Size Dependence of Surface Tension. The effect of curvature on surface tension in capillary condensation is an unresolved issue: some researchers have introduced the curvature-dependent surface tension in the modeling works,[30−34,36,38,41,51] while other researchers have neglected the effect.[10,26−29,35,37,42,44] The present results clearly indicate that the effect is negligibly small for mesopores above ~7 nm in diameter but certainly recognized for smaller mesopores. Furthermore, the combined results for MCM-41 and SBA-12 with small mesopores imply that in such small mesopores, the effect of confinement on the surface tension with respect to the flat surface reverses with temperature. Very recently, Bruot and Caupin[52] reported the temperature effect on the curvature dependence of liquid−vapor surface tension from experiments on nucleation of bubbles in ethanol and n-heptane. The sign of the effect reversed with temperature: the ratio of the surface tensions between the bubble and the flat surface becomes progressively larger with increasing temperature and exceeds unity at higher temperatures. Since ethanol and n-heptane are not unusual substances, a similar temperature effect on the curvature dependence of surface tension for nanobubbles may be conceivable for other molecular liquids like nitrogen. For bubbles and droplets, the curvature is inversely proportional to the size. So, we will consider the effect of pore size on surface tension. From the analogy with their results, we inferred the following equation for the pore-size dependence on the surface tension between the vapor and adsorbed phases.

$$\sigma(R_w, T) = \sigma_\infty/[1 + 0.05/R_w + (-0.03T + 2.3)/R_w{}^2] \tag{12}$$

where $\sigma(R_w, T)$ and σ_∞ are the surface tension of a confined liquid inside a mesopore of radius R_w in nm and a bulk liquid,

respectively, and T is temperature in K. The parameters of eq 12 were determined by trial and error, although they are concerned with the Tolman length and a quantity given by the Tolman length, the bending rigidity constant, the rigidity constant associated with Gaussian curvature, and the surface tension of a flat surface, respectively .[53]

Figure 4 shows a comparison of the re-calculated temperature dependences of the capillary condensation and evaporation
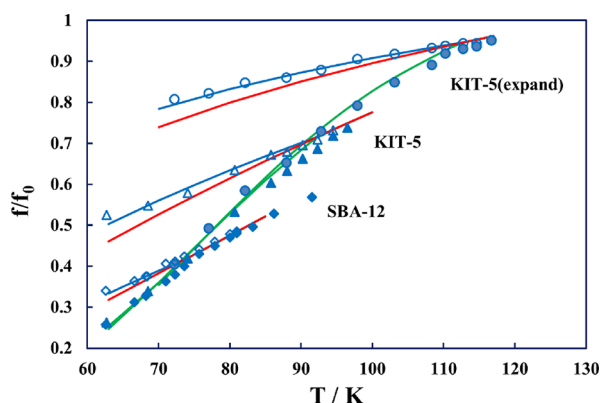

Figure 4. Temperature dependence of the capillary condensation and evaporation pressures (f/f_0) of nitrogen in SBA-12, KIT-5, and KIT-5 (expand). Open and closed symbols denote capillary condensation and evaporation pressures, respectively. Blue, red, and green lines denote the capillary condensation, equilibrium transition, and cavitation pressures, respectively, of nitrogen calculated on the basis of the semimacroscopic model with a size effect in surface tension for a spherical pore.

pressures for spherical pores with the experiments. Here, the capillary condensation and evaporation pressures were re-calculated using the pore-size-dependent surface tension. A fit between theory and experiment for SBA-12 with small spherical mesopores is obviously improved. This further confirms the mechanisms of capillary condensation and evaporation in ink-bottle pores predicted by the previous simulation and thermodynamical modeling studies.[13,19,44,47,48] For cavitation of liquid nitrogen confined to spheroidal pores of mesoporous silicas, Rasmussen et al. have obtained the relationships between the cavitation pressure and the nucleation barrier of cavitation on the pore size based on the MC simulation and experiments.[45] The cavitation pressure depended on the pore size for the samples with pores smaller than ∼11 nm in diameter and remained practically unchanged for the samples with larger pores. Exploiting the correlation between the experimental cavitation pressure and the simulated nucleation barrier, they found that the nucleation barrier increased almost linearly from ∼40 to ∼70 k_bT in the range of pores from ∼7 to ∼11 nm, and varied in narrow diapason of 70−75 k_bT in larger pores.

Figure 5 shows a similar comparison of the temperature dependences of the capillary condensation and evaporation pressures of nitrogen re-calculated for cylindrical pores with several different pore sizes using the pore-size-dependent surface tension with the experiments. The temperature dependence of the vaporlike spinodal is also included in the figure. For an open-ended cylindrical pore, the previous theoretical and simulation studies[6,10,12,39,40] suggest that capillary condensation should take place between the spinodal and equilibrium, whereas capillary evaporation occurs near the point of equilibrium. Neimark et al.[39] have distinguished two hysteresis regimes
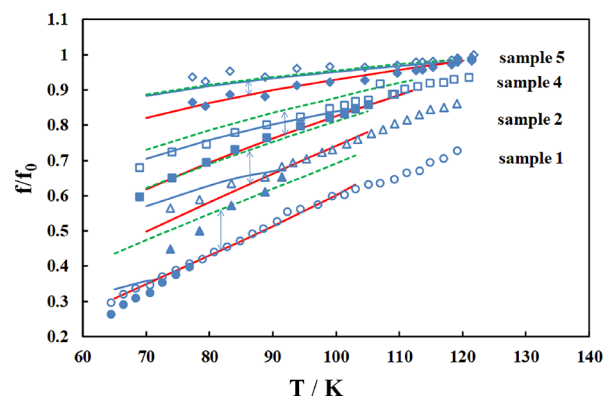

Figure 5. Temperature dependence of the capillary condensation and evaporation pressures (f/f_0) of nitrogen in MCM-41 (sample 1), SBA-15 (sample 2), SBA-15 (sample 4), and SBA-15 (sample 5). Open and closed symbols denote capillary condensation and evaporation pressures, respectively. Blue and red lines denote the capillary condensation and equilibrium transition pressures, respectively, of nitrogen calculated on the basis of the semimacroscopic model with a size effect in surface tension for a cylindrical pore, while green dotted lines denote the vaporlike spinodal pressures of nitrogen calculated.

depending on the pore size: "developed hysteresis" in larger mesopores when condensation occurs close to the vapor−liquid spinodal and "developing hysteresis" when condensation occurs in between the spinodal and equilibrium with a narrower hysteresis loop. For sample 5, the capillary condensation pressures calculated were nearly identical to the vaporlike spinodal pressures in the whole temperature region of hysteresis. The hysteresis observed for sample 5 belongs to the developed hysteresis. For sample 4, on the other hand, the capillary condensation pressures calculated were well below the vaporlike spinodal pressures, although the former approaches the latter with decreasing temperature. The hysteresis observed for sample 4 belongs to the developing hysteresis. Such a classification cannot be applied to the hysteresis observed for samples 1 and 2 because these materials have pore imperfections, and thus the mechanism of the hysteresis is different from that for an ideal cylindrical pore. For the reversible capillary condensation pressures in the relatively small cylindrical mesopores of MCM-41 and SBA-15, a fit between theory and experiment is also improved. The effect of pore size on the surface tension between the vapor and adsorbed phases surely exists. The effect with respect to a flat surface reverses with temperature.

Figure 6 shows a comparison between theory and experiment for a series of the ordered mesoporous silicas with cylindrical pores reported separately in our previous study.[23] The capillary condensation and evaporation pressures calculated based on cylindrical pores were obtained using the pore-size dependent surface tension. Here, MCM-41 (C16) was prepared using an ionic surfactant of shorter chain length as a structure-directing agent as compared to MCM-41 (sample 1). SBA-15 (P85) was prepared using Pluronic P85 as a structure-directing agent, in order to obtain a sample of a smaller pore size. SBA-15 (P123) was prepared using Pluronic P123 and hydrothermally treated at 373 K for 6 days, in order to enlarge the pore size. The hydrothermal treatment time at 373 K of SBA-15 (P85) was only 1 day. In calculations of activated condensation and equilibrium transition pressures, the pore radii of MCM-41 (C16), SBA-15 (P85), and SBA-15 (P123) were assumed to be 1.9, 2.8, and 4.2 nm, respectively. As stated above, the theoretical
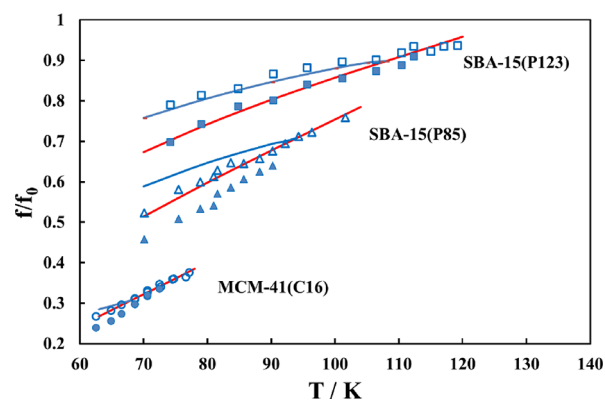
Figure 6. Temperature dependence of the capillary condensation and evaporation pressures (f/f_0) of nitrogen in MCM-41 (C16), SBA-15 (P85), and SBA-15 (P123). Open and closed symbols denote capillary condensation and evaporation pressures, respectively. Blue and red lines denote the capillary condensation and equilibrium transition pressures, respectively, of nitrogen calculated on the basis of the semimacroscopic model with a size effect in surface tension for a cylindrical pore.

and simulation studies for an open-ended cylindrical pore predict that capillary condensation takes place from a metastable multilayer film, while capillary evaporation takes place via a receding meniscus from pore ends at the equilibrium transition pressure.[6,10,12,39,40] Figures 5 and 6 clearly indicate that the temperature dependence of the adsorption hysteresis observed for SBA-15 with mesopores of diameters above ∼7 nm confirms such theoretical predictions for a cylindrical pore. Very recently, Dantas et al.[54] have examined the temperature dependence of the adsorption hysteresis due to capillary condensation of CO_2 in CMK-3-ordered mesoporous carbon using experiments and molecular simulations, where the nucleation barriers for the condensation were estimated from continuous gauge cell Monte Carlo isotherms. They were able to account for the temperature dependence of the adsorption hysteresis by assuming a certain critical nucleation barrier, namely, the level of surmountable nucleation barrier in the present study. In our opinion, the level (∼60 $k_b T$) of surmountable nucleation barrier determined here can give equally a reasonable account for the temperature dependence of the adsorption hysteresis of CO_2, although the value estimated by them was 43 $k_b T$.

For SBA-15 and MCM-41 with smaller mesopore sizes, however, the capillary evaporation pressures in the hysteretic isotherms no longer obey the temperature dependence of the equilibrium transition pressure expected for an ideal cylindrical pore. Instead, the capillary condensation pressures in the hysteretic isotherms are close to the equilibrium transition pressures expected for ideal cylindrical pores. The results are directly concerned with the long-term debate as to which branch of adsorption or desorption is better suited for the pore size analysis of mesoporous materials with cylindrical pores.[5,8,55,56] The capillary evaporation pressures observed are always lower than the equilibrium desorption pressures expected for the ideal cylindrical pore. The presence of the pore corrugation in these ordered mesoporous silicas with cylindrical pores may be responsible for it: minimal deviations from geometric ideality dramatically change the mechanisms of capillary condensation and evaporation. Cavitation or pore-blocking-controlled desorption may occur.

2.4. Pore Imperfections. Effects of the pore imperfections on capillary condensation and evaporation in cylindrical pores have been extensively investigated by experiments,[9,25,50,57−63] theories,[64−68] and simulations.[69−73] It is generally accepted that among various forms of the imperfections, the presence of pore corrugation inside the main channels has considerable effect on the adsorption hysteresis in the ordered mesoporous silicas with cylindrical pores. Here, the pore corrugation is undulations along the pore axis. "Advanced adsorption" and "single pore blocking" are considered for adsorption and desorption, respectively, of a fluid in the corrugated pores.[57,59] In the advanced adsorption, the condensation in narrow sections of the pores triggers or advances the condensation in the neighboring wide sections. In the single pore blocking, the liquids remained in the narrow sections block the desorption of the liquids condensed in the wide sections located at a deeper position upon desorption. However, the exact nature of the pore imperfections that affect the adsorption hysteresis in the ordered mesoporous silicas with cylindrical pores is still unclear. To better understand it, we compared the temperature dependences of the adsorption hysteresis for nitrogen in the two kinds of SBA-15, SBA-15 (sample 2) and SBA-15 (P85), with those calculated for ideal cylindrical pores of several different pore radii. Figures 7 and 8
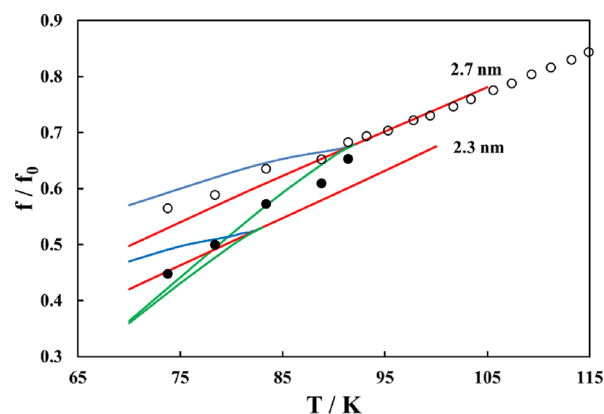

Figure 7. Comparison of the capillary condensation and evaporation pressures (f/f_0) of nitrogen in SBA-15 (sample 2) with the theoretical estimation for two kinds of cylindrical pores with different radii. Open and closed circles denote capillary condensation and evaporation pressures, respectively. Blue, red, and green lines denote the capillary condensation, equilibrium transition, and cavitation pressures, respectively, of nitrogen calculated on the basis of the semimacroscopic model with a size effect in surface tension for cylindrical pores.

show such comparisons for SBA-15 (sample 2) and SBA-15 (P85), respectively. Three theoretical dependences for each pore size were calculated for activated condensation, equilibrium transition, and activated evaporation. For an ideal cylindrical pore, the activated capillary condensation and activated evaporation pressures merge with the equilibrium transition pressure above T_h. This means that above T_h, the capillary condensation and evaporation of a fluid in a particular section of the corrugated cylindrical pore do not at all depend on the state of the neighboring section and occur reversibly at a particular pressure depending only on the strength of confinement of the section. Below T_h, the advanced adsorption on adsorption and the single pore blocking or cavitation on desorption begin to occur in the corrugated pores. The capillary condensation occurs first in small pore sections followed by the growth of the liquid bridges near the equilibrium transition
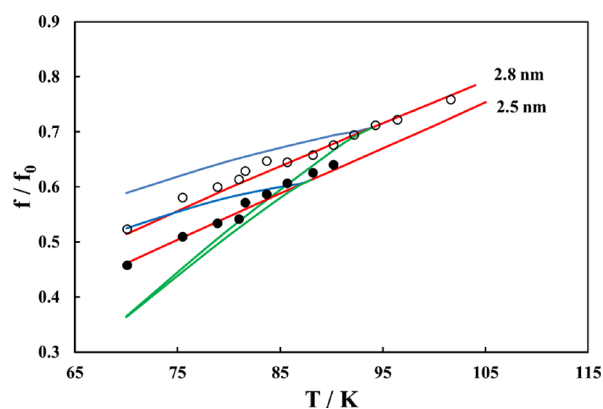
Figure 8. Comparison of the capillary condensation and evaporation pressures (f/f_0) of nitrogen in SBA-15 (P85) with the theoretical estimation for two kinds of cylindrical pores with different radii. Open and closed circles denote capillary condensation and evaporation pressures, respectively. Blue, red, and green lines denote the capillary condensation, equilibrium transition, and cavitation pressures, respectively, of nitrogen calculated on the basis of the semimacroscopic model with a size effect in surface tension for cylindrical pores.

pressures of individual sections. Therefore, the capillary condensation is expected to occur near the equilibrium transition pressures of the individual sections of the corrugated pores, in accord with the conclusion of a very recent study.[18]

As Figures 7 and 8 show, the capillary condensation of nitrogen in the corrugated pores of the ordered mesoporous silicas takes place near the equilibrium transition pressure rather than the activated condensation, in accord with such an expectation. On the other hand, the capillary evaporation is expected to occur via pore blocking or cavitation at pressures lower than the equilibrium. For SBA-15 (P85), the capillary evaporation pressure in the hysteretic isotherms obeys the temperature dependence of the equilibrium transition pressure expected for a cylindrical pore of 2.5 nm in radius smaller than the average pore radius of 2.8 nm. This agrees with the desorption behavior solely controlled by the pore blocking, where most of the liquid condensed inside the corrugated pores can desorb through the equilibrium desorption of liquids condensed in narrow sections close to both pore ends. For the corrugated pores, the radius of each section within a given pore is supposed to follow a normal distribution with its mean radius and standard deviation $\sigma_{section}$.[67] Due to the random distribution of the section radii and the relatively long pore, it is expected that the differences between the radii of the narrow sections close to the pore ends and the mean radius are larger than $\sigma_{section}$. For the pore corrugation of SBA-15, the value of $\sigma_{section}$ slightly smaller than ~0.3 nm is plausible for the mean radius of 2.8 nm.[67] For SBA-15 (sample 2), on the other hand, the desorption in the hysteretic isotherms seems to proceed by cavitation because the capillary evaporation pressure obeys the temperature dependence of the activated evaporation pressure calculated. The radii of the narrow sections close to the pore ends are estimated to be close to ~2.3 nm, while the mean radius is 2.7 nm. The corrugation amplitude of SBA-15 (sample 2) is slightly larger than that of SBA-15 (P85).

It is generally believed that the pore imperfections of MCM-41 are less than SBA-15. However, the present two samples of MCM-41, MCM-41 (sample 1) and MCM-41 (C16), showed thermal behavior of hysteresis loops typical of the corrugated cylindrical pores. The capillary condensation pressure in the

hysteretic isotherms obeys the temperature dependence of the equilibrium transition pressure expected for an ideal cylindrical pore, while the capillary evaporation pressure deviates from the equilibrium transition pressure. Even a smaller amplitude of the pore corrugation in MCM-41 can affect considerably the adsorption hysteresis because the mean radius of the channels is also smaller than SBA-15. This has been revealed in our previous study of modeling calculations.[67] We have previously reported that MCM-41 carefully synthesized shows the temperature dependence of the adsorption hysteresis typical of an ideal cylindrical pore.[25] The effect of the pore corrugation on the adsorption hysteresis depends on the synthesis method rather than the kind of the ordered mesoporous silica. All these studies clearly indicate that for mesoporous materials with cylindrical pores, a routine selection of the desorption branch for pore size analysis is not always validated because it is not confirmed that the desorption process is associated with the equilibrium vapor–liquid transition in all instances.

3. CONCLUSIONS

The present continuum models capture the exact nature of capillary condensation and evaporation phenomena of nitrogen in cagelike and cylindrical pores with ideal geometries. The effect of curvature on the surface tension in capillary condensation is negligibly small for mesopores of diameters above ~7 nm but cannot be neglected for mesopores of smaller sizes. The effect of pore size on the surface tension with respect to a flat surface reverses with temperature. For SBA-15 with cylindrical mesopores of diameters above ~7 nm, the temperature dependences of the adsorption hysteresis measured confirm the previous theoretical predictions concerning the mechanisms of capillary condensation and evaporation in an ideal cylindrical pore. For SBA-15 and MCM-41 with smaller mesopore sizes, on the other hand, the capillary condensation takes place close to the equilibrium transition pressures, while the capillary evaporation takes place at pressures lower than the equilibrium, as opposed to the theoretical predictions, owing to single pore blocking. A change in the mechanisms of capillary condensation and evaporation is ascribable to the corrugation of the cylindrical pores. The effect of the pore corrugation on the adsorption hysteresis depends on the synthesis method rather than the kind of the ordered mesoporous silica.

For materials with open-ended cylindrical pores of minor imperfections, the classical scenario is confirmed: the desorption branch is equilibrium, and the adsorption branch corresponds to the delayed (activated) capillary condensation transitions through the nucleation of a capillary bridge. For materials with pore blocking or pore wall corrugations, the desorption transition is shifted to the pressures smaller than the equilibrium pressure, which is most pronounced due to possible cavitation when the blocking pores are small.

4. MATERIALS AND METHODS

4.1. Materials. Three kinds of ordered mesoporous silicas with cagelike pores (KIT-5, KIT-5 (expand), and SBA-12) and seven kinds of ordered mesoporous silicas with cylindrical pores (MCM-41 (sample 1), SBA-15 (sample 2), SBA-15 (sample 4), SBA-15 (sample 5), MCM-41 (C16), SBA-15 (P85), and SBA-15 (P123)) were used in the study. Sample synthesis and characterization were described elsewhere.[23,24]

4.2. Measurement and Data Treatment. Measurements of adsorption isotherms were also described in detail else-

where.[23,24] Capillary condensation and evaporation pressures of nitrogen in the ordered mesoporous silicas at various temperatures were reproduced from our previous studies.[23,24] The condensation and evaporation pressures were transformed to fugacities using the second and third virial coefficients,[74] in order to compare with theoretical results.

4.3. Spherical Pore. As the vapor pressure increases, the fluid is progressively adsorbed at the pore wall owing to a fluid–solid interaction, forming a multilayer film, which bounds a vapor "bubble" in the pore core. In the framework of the same thermodynamic approach as that used for a cylindrical pore,[37,42] the grand potential of the spherical bubble of radius R, per unit pore, with respect to the completely filled pore is

$$\Omega(R) = 4\pi \int_0^R r\sqrt{R^2 - r^2}\, (P_l(r) - P_g(r))\, dr + 4\pi\sigma R^2 \tag{1}$$

where $P_l(r)$ and $P_g(r)$ are the local liquid and gas pressures, respectively, and σ is the liquid–vapor surface tension. For small undersaturations, $P_l(r)$ and $P_g(r)$ satisfy the relation[42,75]

$$P_l(r) - P_g(r) = (\rho_l(P_{sat}) - \rho_g(P_{sat}))(\mu_g(P^\infty_g)$$
$$- \mu_g(P_{sat}) - U(r))$$
$$= \Delta\rho(\Delta\mu - U(r)) \tag{2}$$

where $\rho_l(P_{sat})$ and $\rho_g(P_{sat})$ are densities of bulk liquid and vapor at saturation, respectively, $\mu_g(P^\infty_g)$ and $\mu_g(P_{sat})$ are chemical potentials of external vapor in contact with a solid and saturated vapor, respectively, and $U(r)$ is a solid–fluid interaction potential. The solid–fluid interaction potential for silica spherical pore is adopted from that used frequently in the molecular simulation works.[13,19] A distance between the surface of the pore wall and the pore center, R_w, is usually referred to as the pore radius, while a distance between the centers of oxygen atoms in the first layer of the pore wall and the pore center, R_0, is used in the solid–fluid potential function. Two distances have a relation $R_0 = R_w + \sigma_{ss}/2$, where σ_{ss} is the interaction parameter for oxygen atom. Introducing the reduced radius $x = R/R_0$, the grand potential of the spherical bubble of radius x, per one pore, with respect to the completely filled pore is given by a combination of eqs 1 and 2 as follows:

$$\Omega(x) = \frac{4}{3}\Delta\rho\Delta\mu\pi R_0^3 x^3 + 4\pi\sigma R_0^2 x^2 - 8\pi 2\Delta\rho R_0^3 \rho_s \varepsilon_{sf}\sigma_{sf}^2$$
$$\int_0^x y\sqrt{x^2 - y^2}\, F(y, R_0)\, dy \tag{3}$$

$$F(x, R0) = \frac{2}{5} \sum_{i=0}^9 \left[\left(\frac{\sigma_{sf}}{R_0}\right)^{10} (1 - x)^{i-10} + (-1)^{2i-10} \right.$$
$$\left(\frac{\sigma_{sf}}{R_0}\right)^{10} (1 + x)^{i-10} \right]$$
$$- \sum_{i=0}^3 \left[\left(\frac{\sigma_{sf}}{R_0}\right)^4 (1 - x)^{i-4} + (-1)^{2i-4}\left(\frac{\sigma_{sf}}{R_0}\right)^4 \right.$$
$$(1 + x)^{i-4} \right] \tag{4}$$

where ρ_s is the number density of oxygen atoms, σ_{sf} and ε_{sf} are the fluid–solid interaction parameters. Equilibrium conditions $(d\Omega(x)/dx = 0, \Omega(x) = 0)$ lead to

$$-x_{eq} + \frac{3}{x_{eq}} \frac{2\pi\Delta\rho R_0\rho_s\varepsilon_{sf}\sigma_{sf}^2}{\sigma} \int_0^{x_{eq}} y\sqrt{x_{eq}^2 - y^2}$$
$$F(y, R_0)\, dy - \frac{2\pi\Delta\rho R_0\rho_s\varepsilon_{sf}\sigma_{sf}^2}{\sigma} \frac{d}{dx}$$
$$\left[\int_0^{x_{eq}} y\sqrt{x_{eq}^2 - y^2}\, F(y, R_0)\, dy \right]$$
$$= 0 \tag{5}$$

where x_{eq} is reduced radius at equilibrium. x_{eq} is obtained by solving eq 5 with a bisection method. Then, the equilibrium condensation pressure (relative fugacity f/f_0) can be calculated using x_{eq} and the equilibrium condition $\Omega(x) = 0$. The parameters of the fluid–solid interactions are taken from previous works as follows: $\sigma_{sf} = 3.17$ Å, $\varepsilon_{sf}/k_b = 147.3$ K, $\rho_s = 0.153$ Å^{-2}, and $\sigma_{ss} = 2.726$ Å.[13,41] The difference of liquid and vapor densities $(\Delta\rho)$ and surface tension (σ) for bulk liquid are taken from ref 42.

Mechanisms of liquid and vapor nucleation in a spherical pore are straightforward.[44] Capillary condensation takes place when the energy barrier between the maximum and minimum of the grand potential becomes surmountable, while capillary evaporation takes place when the energy barrier at the maximum of the grand potential becomes surmountable. Dimensionless energy barrier heights for liquid nucleation (E_l^*) and vapor nucleation (cavitation) (E_v^*) are given by the following two equations 6 and 7, respectively.

$$\frac{E_l^*}{4\pi\sigma R_0^2} = \frac{2\pi\Delta\rho R_0\rho_s\varepsilon_{sf}\sigma_{sf}^2}{\sigma} \left[\int_0^{x_m} y\sqrt{x_m^2 - y^2}\, F(y, R_0)\, dy \right.$$
$$\left. - \int_0^{x_t} y\sqrt{x_t^2 - y^2}\, F(y, R_0)\, dy \right]$$
$$- \frac{R_0\Delta\rho k_b\, T\ln\left(\frac{f}{f_0}\right)}{3\sigma} (x_m^3 - x_t^3) + x_t^2 - x_m^2 \tag{6}$$

$$\frac{E_v^*}{4\pi\sigma R_0^2} = \frac{R_0\Delta\rho k_b\, T\ln\left(\frac{f}{f_0}\right)}{3\sigma} x_t^3 - \frac{2\pi\Delta\rho R_0\rho_s\varepsilon_{sf}\sigma_{sf}^2}{\sigma}$$
$$\int_0^{x_t} y\sqrt{x_t^2 - y^2}\, F(y, R_0)\, dy + x_t^2 \tag{7}$$

where x_t and x_m are the reduced radii at energy maximum and minimum and f and f_0 are the fugacities of external gas and saturated gas, respectively. When the nucleation barrier is surmounted by thermal energy, capillary condensation and evaporation occur.

At a pressure higher than the equilibrium, activated condensation occurs. The nucleation barriers can be calculated as a function of relative fugacity pressure (f/f_0) for given temperature and pore size. Then, equilibrium transition, activated condensation, and activated evaporation (cavitation) pressures are obtained from a comparison between the curve of the normalized energy barrier versus f/f_0 and the normalized level of surmountable nucleation barrier.

4.4. Cylindrical Pore. In the framework of a continuum thermodynamic approach, the grand potential of the cylindrical bubble of radius R, per unit pore length, with respect to the completely filled pore is[42]

$$\Omega(R) = 2\pi \int_0^R r\Delta\rho(\Delta\mu - U(r))\,\mathrm{d}r + 2\pi\sigma R \tag{8}$$

BW used the interaction potential of Saam and Cole (SC)[28] for $U(r)$. However, this choice of the interaction potential leads to large discrepancies in T_h between theory[42] and experiment[24] for nitrogen in the ordered mesoporous silicas with cylindrical pores. Ustinov and Do (UD)[37] have derived the fluid–solid potential for nitrogen in cylindrical and spherical pores of silica from the potential exerted by the flat surface of a reference nonporous silica in the framework of the continuum approach. The potential of SC is significantly weaker than that of UD in the region of the pore core, where capillary condensation takes place. Instead, we employ a potential function of Tjatjopoulos et al.[76] for $U(r)$ because the strength of this potential function is almost the same as that of UD in the region of the pore core. The potential function has been often used in molecular simulation works of capillary condensation in a cylindrical silica pore.[12,55,77] HTM also used this potential function in their modeling work of activated and equilibrium condensation.[41] Introducing the reduced radius $x = R/R_0$, the grand potential of the system is

$$\Omega(x) = \Delta\rho\Delta\mu\pi R_0^2 x^2 + 2\pi\sigma R_0^2 x - 2\pi^3\Delta\rho R_0^2\rho_s\varepsilon_{sf}\sigma_{sf}^2$$
$$\int_0^x yF(y, R_0)\,\mathrm{d}y \tag{9}$$

Here,

$$F(x, R_0) = \frac{63}{32}\left[\frac{R_0}{\sigma_{sf}}(1 - x^2)\right]^{-10} F\left[-\frac{9}{2}, -\frac{9}{2}; 1; x^2\right]$$
$$- 3\left[\frac{R_0}{\sigma_{sf}}(1 - x^2)\right]^{-4} F\left[-\frac{3}{2}, -\frac{3}{2}; 1; x^2\right] \tag{10}$$

where $F(a, b, c; d)$ is a hypergeometric function. Equilibrium capillary condensation (desorption), activated capillary condensation, and activated capillary evaporation (cavitation) pressures can be calculated according to the BW approach.[42] Equilibrium conditions $(\mathrm{d}\Omega(x)/\mathrm{d}x = 0, \Omega(x) = 0)$ leads to

$$\frac{\sigma}{x_{eq}} + R_0\,\Delta\rho\pi^2\rho_s\varepsilon_{sf}\sigma_{sf}^2\left[F(x, R_0) - \frac{2}{x_{eq}^2}\right.$$
$$\int_0^x yF(y, R_0)\,\mathrm{d}y\Bigg]$$
$$= 0 \tag{11}$$

where x_{eq} is reduced radius at equilibrium. x_{eq} is obtained by solving eq 11 with a bisection method. Then, equilibrium condensation pressure can be calculated using x_{eq} and condition $\mathrm{d}\Omega(x)/\mathrm{d}x = 0$.

Capillary condensation takes place through the vapor-to-liquid nucleation via bridging. When capillary evaporation at equilibrium from pore ends is forbidden, it occurs through the liquid-to-vapor nucleation via cavitation.[42] The dimensionless level of surmountable nucleation barrier, $N_c = E^*/k_b T$, is determined as described for the case of an inkbottle pore, where

k_b is the Boltzmann constant. The energy barrier heights of the liquid nucleation and the vapor nucleation as a function of f/f_0 are obtained for given temperature and pore size according to the BW approach.[42] Equilibrium transition, activated condensation, and activated evaporation pressures can be obtained from a comparison between the curve of the normalized energy barrier height vs f/f_0 and the normalized level of surmountable nucleation barrier.

AUTHOR INFORMATION

Corresponding Author

Kunimitsu Morishige − *Department of Chemistry, Okayama University of Science, Okayama 700-0005, Japan;* orcid.org/0000-0003-3874-5115; Email: morishi@chem.ous.ac.jp

Complete contact information is available at:
https://pubs.acs.org/10.1021/acsomega.1c01643

Notes

The author declares no competing financial interest.

REFERENCES

(1) Zafar, U.; Vivacqua, V.; Calvert, G.; Ghadiri, M.; Cleaver, J. A. S. A review of bulk powder caking. *Powder Technol.* **2017**, *313*, 389−401.

(2) Galukhin, A.; Bolmatenkov, D.; Emelianova, A.; Zharov, I.; Gor, G. Y. Porous Structure of Silica Colloidal Crystals. *Langmuir* **2019**, *35*, 2230−2235.

(3) Song, Y.; Davy, C. A.; Troadec, D.; Bourbon, X. Pore network of cement hydrates in a High Performance Concrete by 3D FIB/SEM − Implications for macroscopic fluid transport. *Cem. Concr. Res.* **2019**, *115*, 308−326.

(4) Barsotti, E.; Tan, S. P.; Saraji, S.; Piri, M.; Chen, J.-H. A review on capillary condensation in nanoporous media: Implications for hydrocarbon recovery from tight reservoirs. *Fuel* **2016**, *184*, 344−361.

(5) Horikawa, T.; Do, D. D.; Nicholson, D. Capillary condensation of adsorbates in porous materials. *Adv. Colloid Interface Sci.* **2011**, *169*, 40−58.

(6) Monson, P. A. Understanding adsorption/desorption hysteresis for fluids in mesoporous materials using simple molecular models and classical density functional theory. *Microporous Mesoporous Mater.* **2012**, *160*, 47−66.

(7) Coasne, B.; Galarneau, A.; Pellenq, R. J. M.; Di Renzo, F. Adsorption, intrusion and freezing in porous silica: the view from the nanoscale. *Chem. Soc. Rev.* **2013**, *42*, 4141−4171.

(8) Thommes, M.; Cychosz, K. A. Physical adsorption characterization of nanoporous materials: progress and challenges. *Adsorption* **2014**, *20*, 233−250.

(9) Mistura, G.; Bruschi, L.; Lee, W. Adsorption on Highly Ordered Porous Alumina. *J. Low Temp. Phys.* **2016**, *185*, 138−160.

(10) Broekhoff, J. C. P.; de Boer, J. H. Studies on Pore Systems in Catalysts IX. Calculation of Pore Distributions from the Adsorption Branch of Nitrogen Sorption Isotherms in the Case of Open Cylindrical Pores A. Fundamental Equations. *J. Catal.* **1967**, *9*, 8−14.

(11) Broekhoff, J. C. P.; de Boer, J. H. Studies on Pore Systems in Catalysts XI. Pore Distributions from the Adsorption Branch of a Nitrogen Adsorption Isotherm in the Case of "Ink-Bottle" Type Pores. *J. Catal.* **1968**, *10*, 153−165.

(12) Vishnyakov, A.; Neimark, A. V. Studies of Liquid-Vapor Equilibria, Criticality, and Spinodal Transitions in Nanopores by the Gauge Cell Monte Carlo Simulation Method. *J. Phys. Chem. B* **2001**, *105*, 7009−7020.

(13) Ravikovitch, P. I.; Neimark, A. V. Density Functional Theory of Adsorption in Spherical Cavities and Pore Size Characterization of Templated Nanoporous Silicas with Cubic and Three-Dimensional Hexagonal Structures. *Langmuir* **2002**, *18*, 1550−1560.

(14) Wall, G. C.; Brown, R. J. C. The Determination of Pore-Size Distributions from Sorption Isotherms and Mercury Penetration in Interconnected Pores: The Application of Percolation Theory. *J. Colloid Interface Sci.* **1981**, *82*, 141−149.

(15) Ball, P. C.; Evans, R. Temperature Dependence of Gas Adsorption on a Mesoporous Solid: Capillary Criticality and Hysteresis. *Langmuir* **1989**, *5*, 714−723.

(16) Liu, H.; Zhang, L.; Seaton, N. A. Sorption Hysteresis as a Probe of Pore Structure. *Langmuir* **1993**, *9*, 2576−2582.

(17) Thommes, M.; Smarsly, B.; Groenewolt, M.; Ravikovitch, P. I.; Neimark, A. V. Adsorption Hysteresis of Nitrogen and Argon in Pore Networks and Characterization of Novel Micro- and Mesoporous Silicas. *Langmuir* **2006**, *22*, 756−764.

(18) Bonnet, F.; Melich, M.; Puech, L.; d'Auriac Angelés, J. C.; Wolf, P. E. On Condensation and Evaporation Mechanisms in Disordered Porous Materials. *Langmuir* **2019**, *35*, 5140−5150.

(19) Vishnyakov, A.; Neimark, A. V. Monte Carlo Simulation Test of Pore Blocking Effects. *Langmuir* **2003**, *19*, 3240−3247.

(20) Morishige, K.; Nakamura, Y. Nature of Adsorption and Desorption Branches in Cylindrical Pores. *Langmuir* **2004**, *20*, 4503−4506.

(21) Morishige, K. Adsorption hysteresis in ordered mesoporous silicas. *Adsorption* **2008**, *14*, 157−163.

(22) Morishige, K.; Tateishi, N.; Fukuma, S. Capillary Condensation of Nitrogen in MCM-48 and SBA-16. *J. Phys. Chem. B* **2003**, *107*, 5177−5181.

(23) Morishige, K.; Ishino, M. Lower Closure Point of Adsorption Hysteresis in Ordered Mesoporous Silicas. *Langmuir* **2007**, *23*, 11021−11026.

(24) Morishige, K.; Ito, M. Capillary condensation of nitrogen in MCM-41 and SBA-15. *J. Chem. Phys.* **2002**, *117*, 8036−8041.

(25) Morishige, K. Nature of Adsorption Hysteresis in Cylindrical Pores: Effect of Pore Corrugation. *J. Phys. Chem. C* **2016**, *120*, 22508−22514.

(26) Broekhoff, J. C. P.; de Boer, J. H. Studies on Pore Syestems in Catalysts X. Calculations of Pore Distributions from the Adsorption Branch of Nitrogen Sorption Isotherms in the Case of Open Cylindrical Pores B. Applications. *J. Catal.* **1967**, *9*, 15−27.

(27) Broekhoff, J. C. P.; de Boer, J. H. Studies on Pore Systems in Catalysts XIII. Pore Distributions from the Desorption Branch of a Nitrogen Sorption Isotherm in the Case of Cylindrical Pores B. Applications. *J. Catal.* **1968**, *10*, 377−390.

(28) Saam, W. F.; Cole, M. W. Excitations and thermodynamics for liquid-helium films. *Phys. Rev. B* **1975**, *11*, 1086−1105.

(29) Celestini, F. Capillary condensation within nanopores of various geometries. *Phys. Lett. A* **1997**, *228*, 84−90.

(30) Sonwane, C. G.; Bhatia, S. K. Adsorption in mesopores: A molecular-continuum model with application to MCM-41. *Chem. Eng. Sci.* **1998**, *53*, 3143−3156.

(31) Zhu, H. Y.; Ni, L. A.; Lu, G. Q. A Pore-Size-Dependent Equation of State for Multilayer Adsorption in Cylindrical Mesopores. *Langmuir* **1999**, *15*, 3632−3641.

(32) Miyahara, M.; Kanda, H.; Yoshioka, T.; Okazaki, M. Modeling Capillary Condensation in Cylindrical Nanopores: A Molecular Dynamics Study. *Langmuir* **2000**, *16*, 4293−4299.

(33) Qiao, S. Z.; Bhatia, S. K.; Zhao, X. S. Prediction of multilayer adsorption and capillary condensation phenomena in cylindrical mesopores. *Microporous Mesoporous Mater.* **2003**, *65*, 287−298.

(34) Qiao, S. Z.; Bhatia, S. K.; Nicholson, D. Study of Hexane Adsorption in Nanoporous MCM-41 Silica. *Langmuir* **2004**, *20*, 389−395.

(35) Ustinov, E. A.; Do, D. D.; Jaroniec, M. Equilibrium Adsorption in Cylindrical Mesopores: A Modified Broekhoff and de Boer Theory versus Density Functional Theory. *J. Phys. Chem. B* **2005**, *109*, 1947−1958.

(36) Kowalczyk, P.; Jaroniec, M.; Terzyk, A. P.; Kaneko, K.; Do, D. D. Improvement of the Derjaguin-Broekhoff-de Boer Theory for Capillary Condensation/Evaporation of Nitrogen in Mesoporous Systems and Its Implications for Pore Size Analysis of MCM-41 Silicas and Related Materials. *Langmuir* **2005**, *21*, 1827−1833.

(37) Ustinov, E. A.; Do, D. D. Application of a generalized thermodynamic approach to characterize mesoporous materials. *Colloids Surf., A* **2006**, *272*, 68−81.

(38) Pellenq, R. J. M.; Coasne, B.; Denoyel, R. O.; Coussy, O. Simple Phenomenological Model for Phase Transitions in Confined Geometry. 2. Capillary Condensation/Evaporation in Cylindrical Mesopores. *Langmuir* **2009**, *25*, 1393−1402.

(39) Neimark, A. V.; Ravikovitch, P. I.; Vishnyakov, A. Adsorption hysteresis in nanopores. *Phys. Rev. E* **2000**, *62*, R1493−R1496.

(40) Vishnyakov, A.; Neimark, A. V. Nucleation of liquid bridges and bubbles in nanoscale capillaries. *J. Chem. Phys.* **2003**, *119*, 9755−9764.

(41) Hiratsuka, T.; Tanaka, H.; Miyahara, M. T. Comprehensive Modeling of Capillary Condensation in Open-Ended Nanopores: Equilibrium, Metastability, and Spinodal. *J. Phys. Chem. C* **2017**, *121*, 26877−26886.

(42) Bonnet, F.; Wolf, P. E. Thermally Activated Condensation and Evaporation in Cylindrical Pores. *J. Phys. Chem. C* **2019**, *123*, 1335−1347.

(43) Everett, D. H.; Haynes, J. M. Model Studies of Capillary Condensation I. Cylindrical Pore Model with Zero Contact Angle. *J. Colloid Interface Sci.* **1972**, *38*, 125−137.

(44) Morishige, K.; Tateishi, N. Adsorption hysteresis in ink-bottle pore. *J. Chem. Phys.* **2003**, *119*, 2301−2306.

(45) Rasmussen, C. J.; Vishnyakov, A.; Thommes, M.; Smarsly, B. M.; Kleitz, F.; Neimark, A. V. Cavitation in Metasatable Liquid Nitrogen Confined to Nanoscale Pores. *Langmuir* **2010**, *26*, 10147−10157.

(46) Lefevre, B.; Saugey, A.; Barrat, J. L.; Bocquet, L.; Charlaix, E.; Gobin, P. F.; Vigier, G. Intrusion and extrusion of water in hydrophobic mesopores. *J. Chem. Phys.* **2004**, *120*, 4927−4938.

(47) Neimark, A. V.; Vishnyakov, A. The birth of a bubble: A molecular simulation study. *J. Chem. Phys.* **2005**, *122*, No. 054707.

(48) Neimark, A. V.; Vishnyakov, A. Phase Transition and Criticality in Small Systems: Vapor-Liquid Transitions in Nanoscale Spherical Cavities. *J. Phys. Chem. B* **2006**, *110*, 9403−9412.

(49) Galarneau, A.; Cambon, H.; Di Renzo, F.; Ryoo, R.; Choi, M.; Fajula, F. Microporosity and connections between pores in SBA-15 mesostructured silicas as a function of the temperature of synthesis. *New J. Chem.* **2003**, *27*, 73−79.

(50) Morishige, K. Effects of Carbon Coating and Pore Corrugation on Capillary Condensation of Nitrogen in SBA-15 Mesoporous Silica. *Langmuir* **2013**, *29*, 11915−11923.

(51) Kim, S.; Kim, D.; Kim, J.; An, S.; Jhe, W. Direct Evidence for Curvature-Dependent Surface Tension in Capillary Condensation: Kelvin Equation at Molecular Scale. *Phys. Rev. X* **2018**, *8*, No. 041046.

(52) Bruot, N.; Caupin, F. Curvature Dependence of the Liquid-Vapor Surface Tension beyond the Tolman Approximation. *Phys. Rev. Lett.* **2016**, *116*, No. 056102.

(53) Block, B. J.; Das, S. K.; Oettel, M.; Virnau, P.; Binder, K. Curvature Dependence of Surface Free Energy of Liquid Drops and Bubbles: A Simulation Study. *J. Chem. Phys.* **2010**, *133*, No. 154702.

(54) Dantas, S.; Struckhoff, K. C.; Thommes, M.; Neimark, A. V. Phase Behavior and Capillary Condensation Hysteresis of Carbon Dioxide in Mesopores. *Langmuir* **2019**, *35*, 11291−11298.

(55) Ravikovitch, P. I.; O'Domhnaill, S. C.; Neimark, A. V.; Schüth, F.; Unger, K. K. Capillary Hysteresis in Nanopores: Theoretical and Experimental Studies of Nitrogen Adsorption on MCM-41. *Langmuir* **1995**, *11*, 4765−4772.

(56) Kruk, M.; Jaroniec, M. Determination of Mesopore Size Distributions from Argon Adsorption Data at 77 K. *J. Phys. Chem. B* **2002**, *106*, 4732−4739.

(57) Kruk, M.; Jaroniec, M.; Sayari, A. Nitrogen Adsorption Study of MCM-41 Molecular Sieves Synthesized Using Hydrothermal Restructuring. *Adsorption* **2000**, *6*, 47−51.

(58) Van Der Voort, P.; Ravikovitch, P. I.; De Jong, K. P.; Benjelloun, M.; Van Bavel, E.; Janssen, A. H.; Neimark, A. V.; Weckhuysen, B. M.; Vansant, E. F. A New Templated Ordered Structure with Combined Micro- and Mesopores and Internal Silica Nanocapsules. *J. Phys. Chem. B* **2002**, *106*, 5873−5877.

(59) Esparza, J. M.; Ojeda, M. L.; Campero, A.; Dominguez, A.; Kornhauser, I.; Rojas, F.; Vidales, A. M.; Lopez, R. H.; Zgrablich, G. N2 sorption scanning behavior of SBA-15 porous substrates. *Colloids and Surfaces A* **2004**, *241*, 35−45.

(60) Tompsett, G. A.; Krogh, L.; Griffin, D. W.; Conner, W. C. Hysteresis and Scanning Behavior of Mesoporous Molecular Sieves. *Langmuir* **2005**, *21*, 8214−8225.

(61) Grosmann, A.; Ortega, C. Nature of Capillary Condensation and Evaporation Processes in Ordered Porous Materials. *Langmuir* **2005**, *21*, 10515−10521.

(62) Bruschi, L.; Mistura, G.; Liu, L.; Lee, W.; Goesele, U.; Coasne, B. Capillary Condensation and Evaporation in Alumina Nanopores with Controlled Modulations. *Langmuir* **2010**, *26*, 11894−11898.

(63) Hitchcock, I.; Lunel, M.; Bakalis, S.; Fletcher, R. S.; Holt, E. M.; Rigby, S. P. Improving sensitivity and accuracy of pore structural characterisation using scanning curves in integrated gas sorption and mercury porosimetry experiments. *J. Colloid Interface Sci.* **2014**, *417*, 88−99.

(64) Androutsopoulos, G. P.; Salmas, C. E. A New Model for Capillary Condensation-Evaporation Hysteresis Based on a Random Corrugated Pore Structure Concept: Prediction of Intrinsic Pore Size Distributions. 1. Model Formulation. *Ind. Eng. Chem. Res.* **2000**, *39*, 3747−3763.

(65) Naumov, S.; Valiullin, R.; Kaegar, J.; Monson, P. A. Understanding adsorption and desorption processes in mesoporous materials with independent disordered channels. *Phys. Rev. E* **2009**, *80*, No. 031607.

(66) Gommes, C. J. Adsorption, Capillary Bridge Formation, and Cavitation in SBA-15 Corrugated Mesopores: A Derjaguin-Broekhoff-de Boer Analysis. *Langmuir* **2012**, *28*, 5101−5115.

(67) Morishige, K. Dependent Domain Model of Cylindrical Pores. *J. Phys. Chem. C* **2017**, *121*, 5099−5107.

(68) Schneider, D.; Valiullin, R. Capillary Condensation and Evaporation in Irregular Channels: Sorption Isotherm for Serially Connected Pore Model. *J. Phys. Chem. C* **2019**, *123*, 16239−16249.

(69) Coasne, B.; Pellenq, R. J.-M. A grand canonical Monte Carlo study of capillary condensation in mesoporous media: Effect of the pore morphology and topology. *J. Chem. Phys.* **2004**, *121*, 3767−3774.

(70) Coasne, B.; Galarneau, A.; Di Renzo, F.; Pellenq, R. J. M. Gas Adsorption in Mesoporous Micelle-Templated Silicas: MCM-41, MCM-48, and SBA-15. *Langmuir* **2006**, *22*, 11097−11105.

(71) Coasne, B.; Galarneau, A.; Di Renzo, F. R. J. M. Effect of Morphological Defects on Gas Adsorption in Nanoporous Silicas. *J. Phys. Chem. C* **2007**, *111*, 15759−15770.

(72) Puibasset, J. Monte-Carlo Multiscale Simulation Study of Argon Adsorption/Desorption Hysteresis in Mesoporous Heterogeneous Tubular Pores like MCM-41 or Oxidized Porous Silicon. *Langmuir* **2009**, *25*, 903−911.

(73) Nguyen, P. T. M.; Do, D. D.; Nicholson, D. On The Cavitation and Pore Blocking in Cylindrical Pores with Simple Connectivity. *J. Phys. Chem. B* **2011**, *115*, 12160−12172.

(74) Boltachev, G. S.; Baidakov, V. G. The Second and Third Virial Coefficients of Simple Fluids. *High Temp.* **2006**, *44*, 83−90.

(75) Evans, R.; Marconi, U. M. B.; Tarazona, P. Capillary Condensation and Adsorption in Cylindrical and Slit-like Pores. *J. Chem. Soc., Faraday Trans. 2* **1986**, *82*, 1763−1787.

(76) Tjatjopoulos, G. J.; Feke, D. L.; Mann, J. A. Molecule-Micropore Interaction Potentials. *J. Phys. Chem.* **1988**, *92*, 4006−4007.

(77) Peng, B.; Yu, Y. X. A Density Functional Theory for Lennard-Jones Fluids in Cylindrical Pores and Its Applications to Adsorption of Nitrogen on MCM-41 Materials. *Langmuir* **2008**, *24*, 12431−12439.